Direct integration of SAW resonators on industrial metal for structural health monitoring applications

P Mengue, Sami Hage-Ali, S Zhgoon, Baptiste Paulmier, Cécile Floer, Florian Bartoli, Omar Elmazria

Direct integration of SAW resonators on industrial metal for Structural Health Monitoring applications

P. Mengue[1*], S. Hage-Ali[1], S. Zghoon[2], Baptiste Paulmier[1], Cécile Floer[1], Florian Bartoli[1] and O. Elmazria[1]

[1]Université de Lorraine, CNRS, IJL, F-54000 Nancy, France

[2]National Research University, Moscow Power Engineering Institute, 14 Krasnokazarmennaja, 111250 Moscow, Russia

E-mail : prince-warol.mengue-m-owono@univ-lorraine.fr, sami.hage-ali@univ-lorraine.fr, omar.elmazria@univ-lorraine.fr

Received xxxxxx
Accepted for publication xxxxxx
Published xxxxxx

Abstract

Surface acoustic wave (SAW) sensors are very promising for structural health monitoring (SHM) applications as they have the advantages of being robust, passive (batteryless), remotely interrogated (wireless) and can even be packageless. This paper describes ultralow-profile surface acoustic wave resonators that can be directly fabricated and integrated on metallic parts in industrial facilities. They are based on piezoelectric thin films (ZnO) which are directly sputtered on polished industrial titanium and stainless steel. With this approach, no sensor glue-bonding to the target is needed, and measurement errors related to this step are avoided. Demonstrator devices have been studied numerically and experimentally. The structural properties of the ZnO thin films were characterized through X-ray diffraction and atomic force microscopy. A preferred orientation (002) was achieved with a roughness of 50 nm on the top surface. Resonators were microfabricated and their functional parameters (i.e. resonance frequency, quality factor and electromechanical coupling) were extracted through impedance measurements and fitted with a Butterworth-Van Dyke (BVD) model. By increasing applied temperatures (up to 450°C) and the strain (up to 1800 με), a linear decrease of the resonance frequency has been shown. A temperature coefficient of frequency (*TCF*) of -46.4 ppm/°C and a good strain sensitivity (1.49 ppm/με) were obtained, thus making the structure promising as a high temperature and strain sensing element in industrial SHM applications.

Keywords: Metal substrate, zinc oxide, Surface Acoustic Wave (SAW), Temperature, strain, sensor, Structure Health Monitoring (SHM).

1. Introduction

Structure monitoring, also known as structure health monitoring (SHM) is a multidisciplinary science whose role is to maintain structures and extend their lifespan by detecting and even predicting faults. The fundamental idea is to equip structures such as bridges, dams, planes and others with a mesh of monitoring devices, very much like the nervous system of a human body, with the goal of anticipating damage and avoid accidents. Data driven systems fueled by the signal processing of multiple sensors are perfectly in line with the technological progress of the industrial revolution 4.0. SHM systems are increasingly popular with manufacturers and institutions in that they are part of economic and preventive strategies. In addition, the low cost, the reduction in size, the autonomy and the permanence of sensors have enabled their popularization which has led to the widening of their field of application. SHM systems typically use many kinds of sensors: optical fibers [1] , various acoustic [2] and ultrasonic sensors, strain gauges and other. Some solutions are quite expensive to implement, while others are not compatible with remote query or with possibly harsh industrial environments.

In this context, Surface Acoustic Wave (SAW) [3] sensors appear particularly interesting. They are made on piezoelectric substrates, namely quartz [4], langasite, lithium niobate and others, on which interdigital transducers (IDTs) and reflectors are patterned. They are sensitive to environmental disturbances (temperature, pressure, strain, and others [5–7]), that create shape and wave velocity changes within the sensor, leading to measurable frequency or time-delay shifts. SAW sensors are fully passive (batteryless) and can be remotely interrogated (wireless), which is paramount for harsh or difficult to reach environments[8].

Conventional SAW sensors are usually bonded with adhesives to the structure or component to be evaluated. The use of organic glue leads to measurement errors due to the partial release of the applied stress and a possible adhesive detachment from the structure. Some examples of SHM SAW sensors that can be found in publications which show the glue failures: Maskay et al. manufactured SAW sensors for wireless operation in harsh environmental conditions at high temperature and exposed to dynamic deformation disturbances by a vibration generator [9], Wilson et al. have developed a SAW deformation sensor for use in the detection of aircraft accessory failures [10]. Oishi et al. performed cantilever vibration studies by combining a vibration sensor, SAW sensor, and pressure sensor to detect structural deterioration [11].

In order to reduce the risk of measurement errors caused by the use of the adhesive, new SAW sensors integrated directly onto metallic structures, without intermediate elements, have been proposed. These sensors are based on the deposition of piezoelectric thin films on metallic parts. Shu et al. [12] investigated a SAW resonator based on an AlN/TC4 structure studied at high temperature [13] and under strain [14], with enhanced sensitivity. These results have shown that SAW sensors directly deposited on a metal substrate can demonstrate good performance and thus be regarded as relevant candidates for a seamless integration in structural health monitoring systems. Another added benefit of this approach is that with appropriate surface protection the total thickness of these sensors remains in the micrometer range, paving the way to their use in extremely space-constrained applications.

This paper investigates ZnO-based micrometer-thick SAW sensors directly integrated onto industrial metal substrates and their use up to 450°C. Initial findings were reported in the conference paper [15]. While the majority of the paper deals with titanium as substrate, some experimental results on stainless steel are also presented to prove the compatibility of this approach with different industrial metals. First, we describe the materials choices, the design, the acoustic FEM modelling, the fabrication process and the structural analysis of the micromachined sensors. Then, the resonator's RF properties for wireless measurements, high temperature sensing up to 450°C and strain measurements up to 1800 με are discussed.

2. Materials choices and numerical modelling

Our choice fell on two resistant metal substrates: titanium which is very light, and stainless steel, which is widely used in the industry. The choice of ZnO as a piezoelectric film is motivated by its ease of growth on almost any substrate, a relatively high electromechanical coupling coefficient (K^2>1%) [16],[17], a temperature sensitivity of -40 ppm/°C, which is convenient for temperature sensing, and a relatively low velocity which allows to envision "packageless" packaging [18],[19].

The base structure in this paper is an Al(IDT)/ZnO/Metal synchronous resonator (Fig. 1). It was initially studied, with Titanium as the metal, using a 3-dimensional finite element analysis (3-D FEM) with the commercial software COMSOL Multiphysics. Due to the periodicity of the SAW structure in the *x*-direction, a unique cell with one metal electrode and antiperiodic conditions is sufficient to provide an approximation of the entire structure (Fig 2a). The physical constants for ZnO and Titanium were taken from the literature and are summarized in Table I. ZnO film constants were validated in the previous work [20]. For aluminum, the constants were directly taken from the Comsol Multiphysics Material library. The wavelength λ is 8μm and the metallization ratio is 50%. Fig. 2b shows the 1D and 3D particle displacement of the fundamental Rayleigh mode at 319.1MHz.

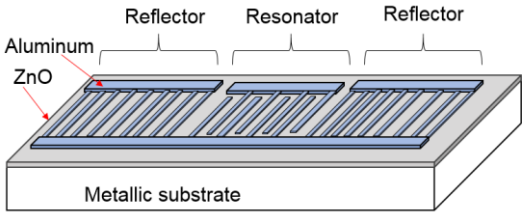

Fig. 1. Schematic view of the one-port SAW resonator.

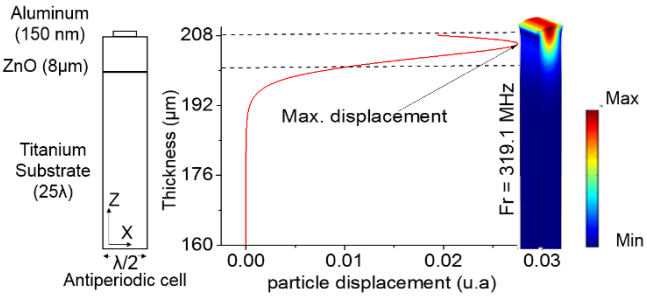

(a) (b)

Fig. 2. Numerical evaluation of the particle displacement in the Al(IDT)/ZnO/Titanium structure.

TABLE I
THE PARAMETERS USED IN THE SIMULATION

Material	**ZnO**	**Titanium**[14]
Density (Kg/m^3)	5680	4510
Elastic constant (GPa)		
C11	209.14	162.2
C12	121.14	91.8
C13	105.359	69
C33	211.194	180.9
C44	423.729	46.7
C66	442.478	35.2
Piezoelectric constant (c/m^2)		
e15	-0.48	…
e31	-0.56	…
e33	1.32	…
Relative permittivity		
ε11	8.54	…
ε33	10.204	…

3. Microfabrication & structural analysis

SAW sensors based on ZnO/Titanium and ZnO/Stainless steel layered structures were fabricated starting from raw metallic plates, intended for regular machining, to prove the compatibility of the approach with industrial materials.

Consequently, a very important step is the surface preparation: the metallic parts (stainless steel and Ti) were first polished with a Struers Tegrapol-3 system, with the aim of obtaining the lowest possible roughness. Different abrasive papers were used followed by the use of a diamond suspension for fine polishing.

Then, 8µm-thick ZnO layers were deposited by RF magnetron sputtering. This ZnO thickness was chosen in order to maximize the wave propagation within the ZnO layer (and not within the potentially lossy metal) in order to reduce the acoustic propagation losses. The deposition parameters were optimized in the previous work [18] and are summarized in Table II.

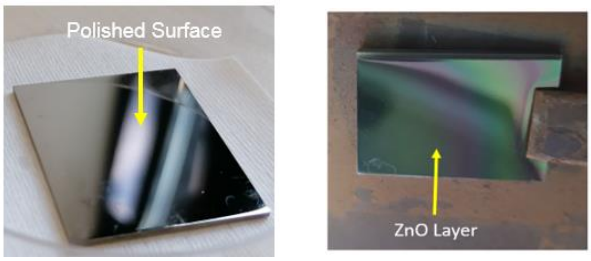

(a) (b)

Fig. 3. a) Top view of the polished surface of titanium (b) with a ZnO film

TABLE II
SUMMARY OF ZNO SPUTTERING PARAMETERS

Target	ZnO (Ø 4-inch)
Gases	8 sccm O_2
	8 sccm Ar
Temperature	170°C
Target power	150 W RF
Total pressure	$3x10^{-3}$ mbar

One-port synchronous SAW resonators were then fabricated. IDTs and reflectors were patterned from a 150 nm thick aluminum layer sputtered on the top surface of the ZnO layer. An optical lithography process with a positive resist and ion beam etching (IBE) was used to etch the aluminum. All the parameters of the Al(IDT)/ZnO/Titanium SAW design are given in Table III.

Fig.4 shows the top view of the one-port SAW resonator achieved on the ZnO/Titanium structure with a well-defined pattern after the microfabrication.

TABLE III
DEVICE DESIGN OF FABRICATED SAW RESONATOR

ZnO thickness	8 µm
Titanium thickness	1 mm
Wavelength on titanium	8 µm
Wavelength on stainless steel	10 µm
Number of IDT finger pairs	100
Number of reflector electrodes	200
Al electrode thickness	150 nm
Aperture (i.e. length of fingers)	271 µm

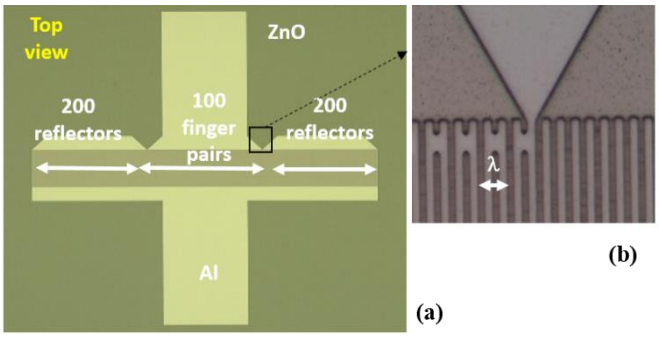

Fig. 4. Top view of the fabricated one-port SAW resonator. Optical full view (a) and zoomed area between the IDT and and a short-circuited reflector obtaind by microscope (b)

The devices were characterized by atomic force microscopy (AFM) to qualify the surface morphology and by X-ray diffraction (XRD) to assess the quality of growth and the orientation of the ZnO thin film. The frequency responses of the resonators were characterized using a RF probe station (Suss Microtec, PM5) and a vector network analyzer (PNA 5230A, Agilent-N5230A).

3. Results and discussion

3.1. Structural and physical characterizations

Fig.5 presents Atomic Force Microscopy (AFM) images of the ZnO/Titanium structure. The root mean square roughness (RMS) of the 8-µm thick ZnO film is 49.29 nm, to be compared with a RMS roughness 20.4 nm of the bare polished titanium.

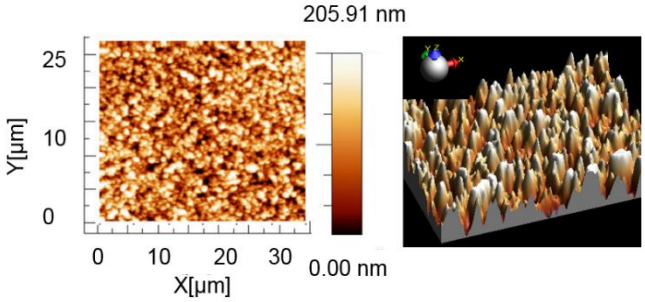

Fig. 5. AFM images of the ZnO growth on Titanium,

The XRD measurements of the ZnO film on both Titanium and Stainless steel substrates are shown in Fig. 6a and Fig.6b, respectively. The graphs show that the ZnO film has a preferred c-axis orientation. The rocking curve of the (002) orientation give a full-width at half-maximum (FWHM) of 4.5° and 2.96° for the Titanium and the Stainless-steel substrate, respectively. These FWHM values are larger than the ones for AlN growth on TC4 Titanium alloy substrate [12] or for ZnO growth on Al foil [21], and are certainly caused by the dispersion of the the ZnO grains orientation in such a high thickness films. Still, they are reasonable for the preparation of surface acoustic waves resonators.

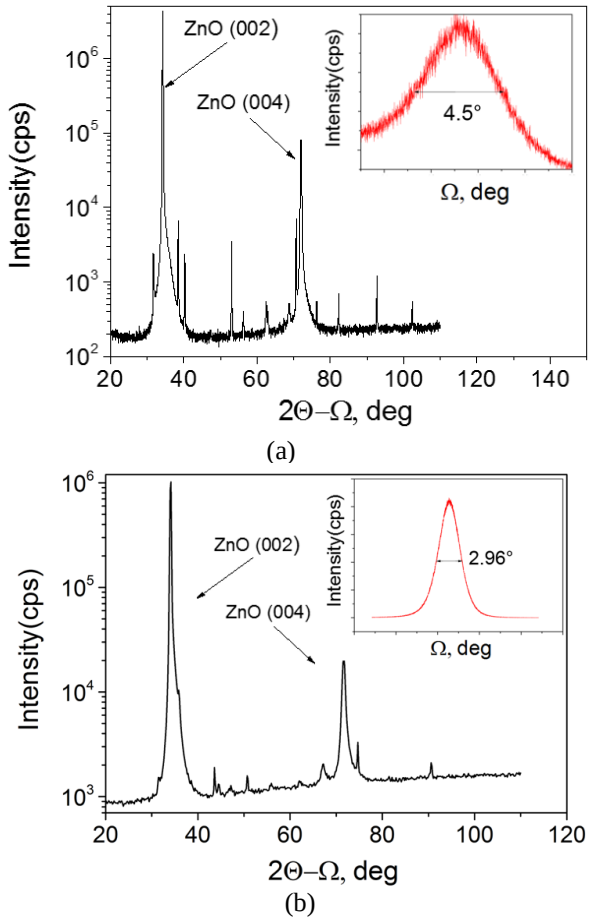

Fig. 6. (a) XRD diagram of the ZnO/Titanium structure. Inset: Rocking curve of the ZnO (002) peak, (b) XRD diagram of the ZnO/Stainless steel structure. Inset: Rocking curve of the ZnO (002) peak

3.2. RF Measurements & resonators parameters extraction

Fig. 7 and Fig. 8 present the S11 measurements of the ZnO/Titanium (λ=8µm) and ZnO/Stainless (λ=10µm) SAW resonators, respectively.

From Fig. 7, the experimental fundamental mode can be identified at 327.52 MHz which is relatively close to the computed value of 319.1 MHz mentioned in Fig. 2.

Fig. 8 shows two peaks where the first one at 263.94 MHz corresponds to the fundamental mode and the second one at 782.115 MHz represents the third harmonic. The 3rd harmonic was only identifiable for the stainless steel resonator.

In both resonators, the 50Ω matching is relatively poor, which can be attributed to the excessive static capacitance between the IDTs and the metallic substrate. The design could be improved impedance-wise with a proper aperture choice.

Another aim of these initial VNA measurements was to extract the resonator parameters namely the electromechanical coupling coefficient K^2, the quality factor Q, and the figure of merit FOM, which is the product of the two, for the ZnO Titanium structure. The goal is to assess if those resonator properties are compatible with a wireless interrogation.

The electromechanical coupling coefficient is usually calculated using the resonant and antiresonant frequencies f_r and f_a , which correspond to the extrema in the admittance modulus |*Y11*|. However, as we can see in the experimental |*Y11*| black curve in Fig. 9, the definition of those extrema is obscured by parasitic peaks, typically caused by stopband ripples below the resonance, and transverse modes around the antiresonance.

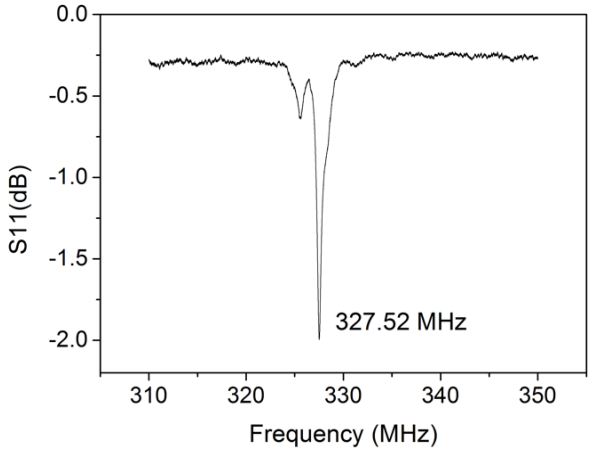

Fig. 7. Experimental reflection coefficient of the ZnO (8µm)/Titanium structure (λ=8µm)

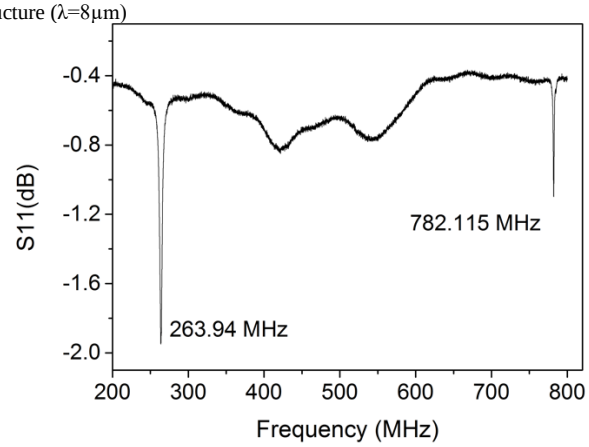

Fig. 8. Experimental reflection coefficient of the ZnO(8µm)/Stainless steel structure (λ=10µm)

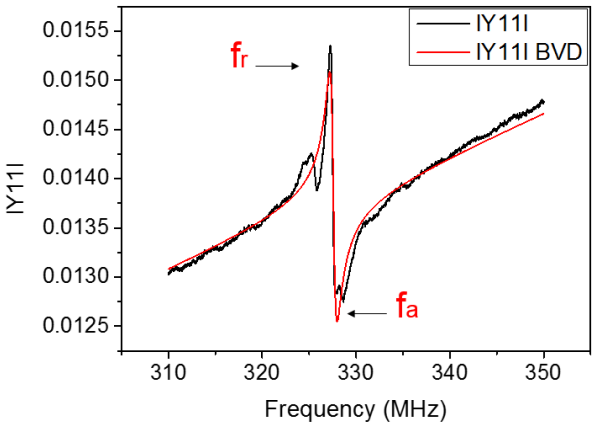

Fig. 9. Admittance curve |*Y11*| (black curve) and the BVD model fitting of |*Y11*| (red curve) for the ZnO/Titanium structure.(λ=8µm)

Hence, the |*Y11*| response of the Al/ZnO/titanium structure was fitted using BVD (Butterworth-Van-Dyke) equivalent circuit of the resonator (Fig. 10) in order to refine the admittance modulus curve and extract the adequate values of the resonance and antiresonance frequencies. The BVD circuit consists of a static capacitance C_0 in parallel with a series $L_mC_mR_m$ resonator corresponding to the motional branch.

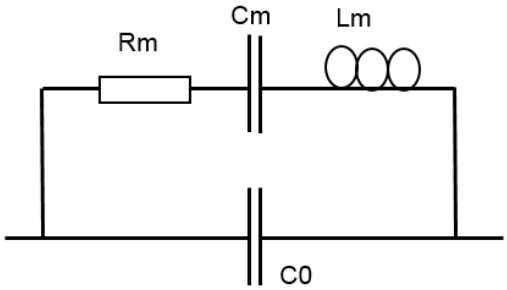

Fig. 10. BVD equivalent circuit.

The BVD model parameters for the ZnO/Titanium SAW resonator at 327.52 MHz and at room temperature (20°C) are estimated in table IV.

Table IV : BVD MODEL PARAMETERS

C0	6.687 pF
Cm	3.022 fF
Rm	388.721 ohm
Lm	0.7813 µH

The effective electromechanical coupling coefficient K^2_{BVD} and the quality factor (Q_{BVD}) are extracted using equation (1) [22] and (2) respectively.

$$K^2{}_{BVD} = K_{C.BVD} = \frac{C_m}{C_0} \qquad (1)$$

$$Q_{BVD} = R_m\sqrt{\frac{L_m}{C_m}} \qquad (2)$$

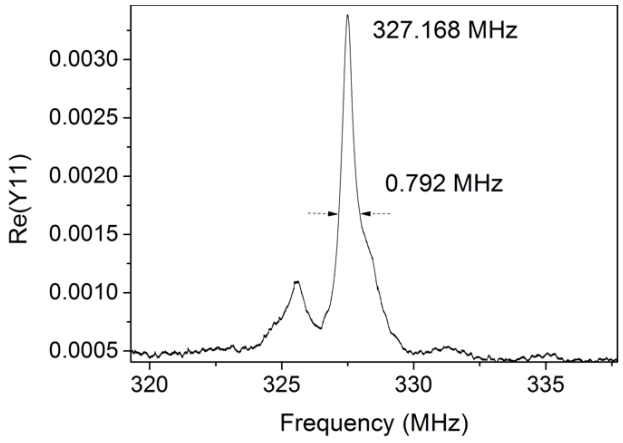

Fig. 11. Measured resonator conductance versus the frequency for the ZnO/Titanium structure

The measured *Q* factor is calculated by the inverse of half-peak fractional bandwidth [23] (see Fig.11) and evaluated at 413.51 for the Titanium/ZnO structure.

TABLE V: ZNO/TITANIUM RESONATOR PARAMETERS

Q measured	413.51
Q_{BVD}	413.64
K^2_{BVD}	0.48%
FOM : $Q_{BVD} \times K^2_{BVD}$	1.987

Table V. summarizes the different extracted parameters for the ZnO/Titanium structure. Measured and BVD-fitted quality factor values are sufficiently close and relatively high (*Q*=413) taking into account that the resonator was made on industrial metal. The BVD-fitted electromechanical coupling coefficient K^2_{BVD} is 0.48%. This value is below the K^2 of ZnO alone (~1%) and is quite expected for such a hybrid structure. The figure of merit *FOM* is very close to 2, proving that the ZnO/Titanium structure exhibits low losses if the ZnO thickness is in the range of λ. According to [22], such *FOM* allows a wireless interrogation with a matched antenna with a re-radiation efficiency of 50%, which is very good and not far from the achievable maximum value (~60%). As result, this resonator is perfectly compatible with remote query.

3.3. High Temperature measurements

To investigate the behavior of our sensors at high temperature, devices were characterized in air atmosphere from the room temperature (20°C) to 450°C. A network analyzer and RF probe station (Signatone Corp, S-1160) equipped with an S-1060 series Signatone thermal probing system was used (Fig.12).

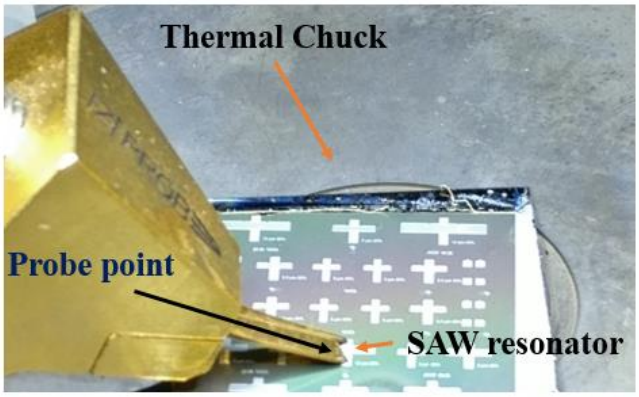

Fig. 12. Measurement of S-parameters with the vector network analyzer (Agilent Technologies,E5061B) at different temperatures.

The *S11* characteristics of ZnO/Titanium resonator measured for various temperature are shown in Fig.13. The resonance frequency decreases linearly when the temperature increases, making the structure suitable for temperature sensing. The temperature coefficient of frequency (*TCF*) (defined in equation (3)) was calculated from Fig. 14 and is approximately equal to -46.4ppm/°C.

$$TCF = \frac{1}{f_r}\frac{\Delta f_r}{\Delta T} \qquad (3)$$

Both heating up to 450°C and cooling cycles were used in measurements and the hysteresis phenomenon can barely be seen. Thus, it proves that the ZnO film behavior is reversible at least up to 450°C.

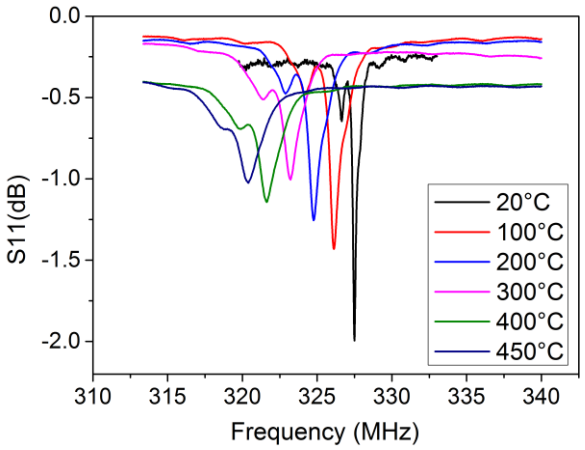

Fig. 13. Reflection coefficient *S11* of ZnO(8µm)/Titanium (λ=8µm) resonator measured from 20°C to 450 °C.

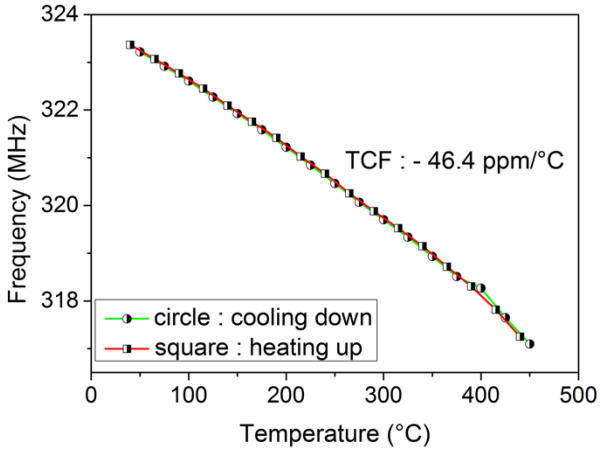

Fig. 14. Frequency of the ZnO/Titanium SAW resonator versus temperature in a heating and cooling cycle

As we can see in Fig.13, the temperature increase somewhat degrades the quality of the S_{11} response. This can be explained by the increase of the electrical conductivity of the semiconducting ZnO film that induces current leakage and thus higher propagation losses [24–26].

Those temperature effects on the electrical characateristics were investigated precisely in terms of resonators parameters. Fig. 15 shows the admittance versus frequency measurements for various temperatures for the ZnO/Titanium structure. After BVD adjustment for each temperature, the extraction of the resonant and antiresonant frequencies led to the determination of the electromechanical coupling coefficients (K^2_{BVD}) and quality factor (Q_{BVD}) using equations (1) and (2) respectively.

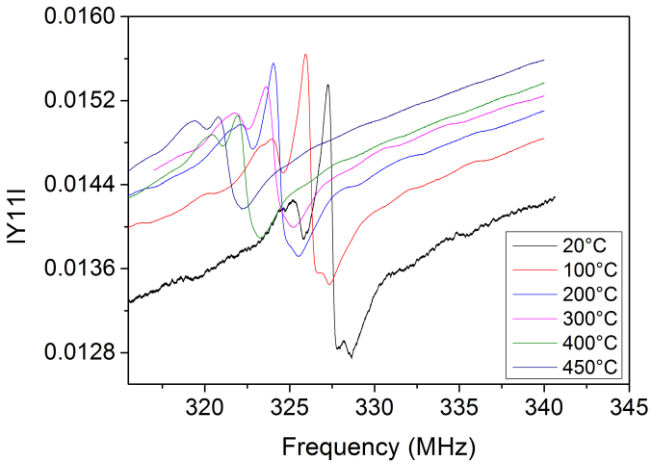

Fig. 15. Temperature evolution of the ZnO/Titanium admittance moduli |*Y11*| from room temperature to 450°C.

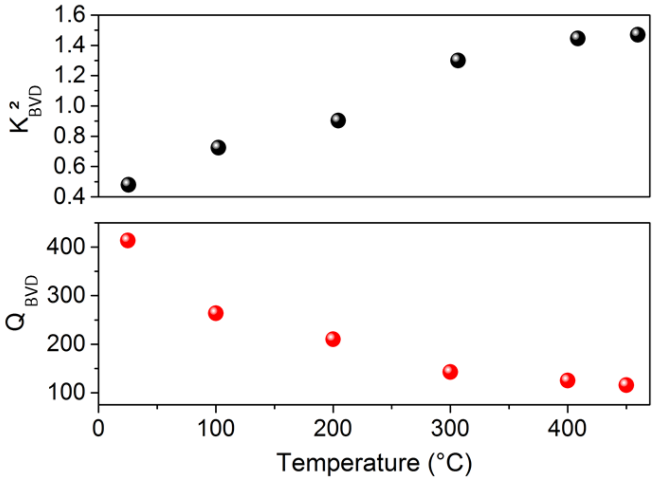

Fig. 16. Electromechanical coupling coefficient K^2 and Quality factor Q of the ZnO/Titanium SAW resonator versus temperature.

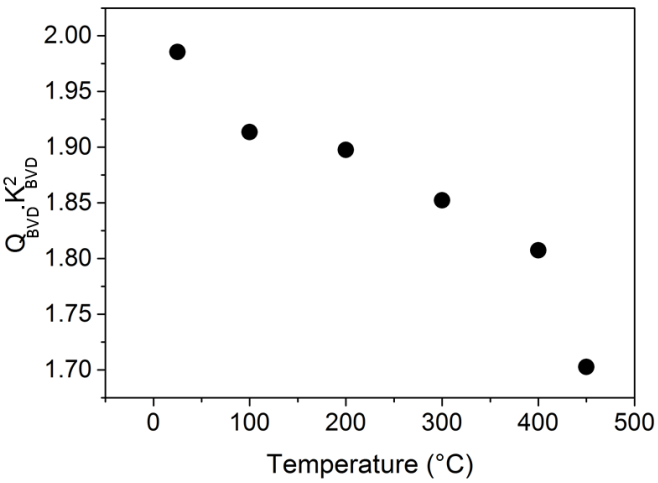

Fig. 17. Figure of merit ($Q_{BVD} \times K^2_{BVD}$) of the ZnO/Titanium SAW resonator versus temperature.

The extracted values from K^2_{BVD}, Q_{BVD} and the figure of merit (Q_{BVD} × K^2_{BVD}) are reported as a function of the temperature in Fig.16 and 17. It can be seen that the K^2_{BVD} values increase when the temperature increases and that the Q_{BVD} values follow an inverse trend down to Q close to 100.

More importantly, the *FOM* decreases from 1.987 to 1.702 when the temperature increases from 20°C to 450°C, which is a quite moderate drop: the structure is still compatible with a wireless interrogation up to 450°C.

3.4. Strain measurements

Experimental three-point bending test was performed in order to evaluate the strain sensitivity of the ZnO (8µm)/titanium structure. The sensor was fabricated directly on a titanium test beam. The beam dimensions are 5mm x 2.5mm x 1mm and a SAW resonator (this time with λ=10µm) is at the center of the beam (see Fig.18a). The 3-points bending testbench is depicted in Fig. 18b.

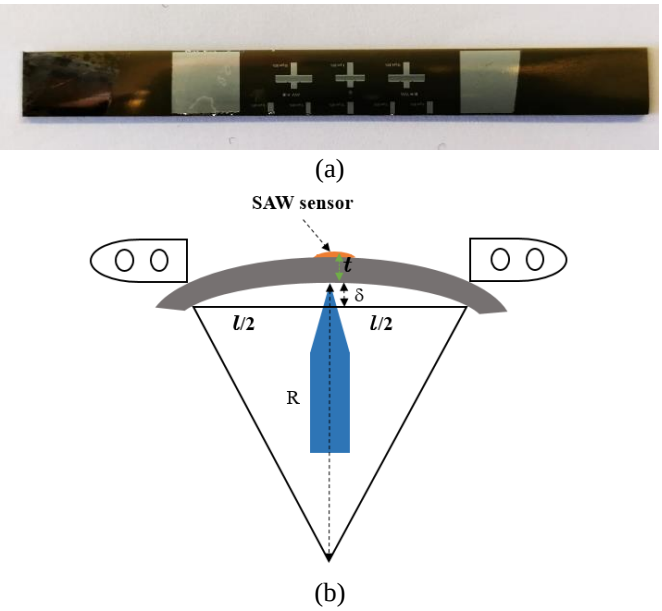

Fig. 18. (a) ZnO(8µm)/Titanium resonator (λ=10µm, center) made on a metallic beam, (b) 3 points bending testbench schematic.

The beam was bent with the bending radius (R), generated by a linear displacement (δ) at the center of the beam. The relationship between bending radius (R) and bending strain (ε) is given in [27].

Fig. 19. shows the central frequency of the device measured under a bending strain from 0 µε to 1800 µε. It can be observed that the frequency increases linearly with the strain. The linear sensitivity of the SAW strain sensor is 1.49 ppm/µε at 25°C. This very good value can be attributed to the direct transmission of the bending stress in the titanium beam to the SAW devices

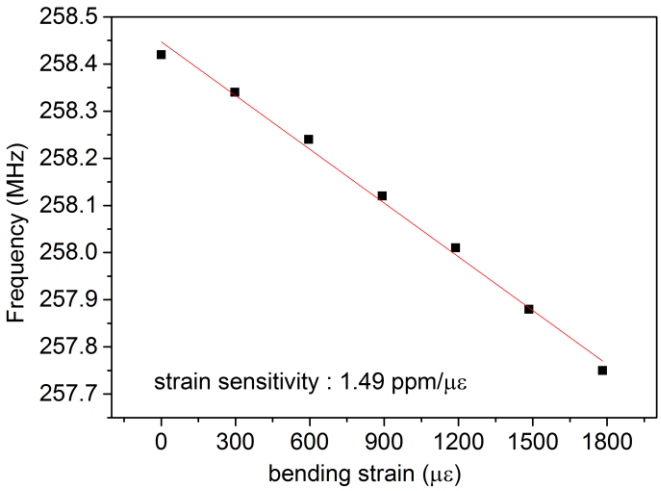

Fig. 19. Resonant frequency versus bending strain

4. Conclusion

In this paper, ZnO/Titanium and ZnO/Stainless steel SAW resonators have been fully studied in order to prove the feasibility of directly integrated SAW devices for SHM application. The direct integration of such sensors on industrial metal using piezoelectric layers allows glue-less assemblies for high temperature and strain measurements, without failures or strain transfer reliability issues typically associated with glue bonding.

Starting from industrial metal, after a key polishing step, good quality SAW resonators were fabricated using fairly standard sputtering and microfabrication. The resonator on ZnO/Titanium exhibits a quality factor of 413 and a figure of merit close to 2. This very good value proves that low-loss SAW resonators, fully compatible with remote query, can be achieved on industrial metal objects. The resonator was measured at high temperatures up to 450°C. It exhibits a linear *TCF* of 46.7 ppm/°C with reversible characteristics, and a moderate figure of merit decrease up to 450°C. Strain measurement using 3 points bending were also performed, showing a very good linear bending strain sensitivity of 1.49 ppm/µε

In summary, those metal integrated SAW sensors are very promising in industrial environments for reliable strain and high temperature SHM measurements with remote query.

Acknowledgements

The authors would like to thank Laurent Badie, Gwladys Lengaigne and Carlos Rojas from MiNaLor cleanroom at Institut Jean Lamour for their help in the fabrication.

The MiNaLor platform is partially supported by FEDER and Grand Est Region through the RaNGE project. This work was supported by Campus France Gabon, the ANR project "SAWGOOD" (ANR-18-CE42-0004-01), the French PIA project "Lorraine Université d'Excellence" (ANR-15-IDEX-04-LUE) and the CAPMAT project ("FEDER-FSE Lorraine et Massif Vosges 2014-2020" and ICEEL).

References

[1] Bastianini F, Matta F, Rizzo A, Galati N and Nanni A Overview of Recent Bridge Monitoring Applications using Distributed Brillouin Fiber Optic Sensors 8

[2] Valentin D and Bunsell A R 2016 A Study of Damage Accumulation in Carbon Fibre Reinforced Epoxy Resin Structures During Mechanical Loading Monitored By Acoustic Emission: *J. Reinf. Plast. Compos.*

[3] Campbell C K 1998 *Surface Acoustic Wave Devices for Mobile and Wireless Communications, Four-Volume Set* (San Diego: Academic Press)

[4] Stoney R, Geraghty D and O'Donnell G E 2014 Characterization of Differentially Measured Strain Using Passive Wireless Surface Acoustic Wave (SAW) Strain Sensors *IEEE Sens. J.* **14** 722–8

[5] Binder A, Bruckner G, Schobernig N and Schmitt D 2013 Wireless Surface Acoustic Wave Pressure and Temperature Sensor With Unique Identification Based on $\rm LiNbO_3$ *IEEE Sens. J.* **13** 1801–5

[6] Scherr H, Scholl G, Seifert F and Weigel R 1996 Quartz pressure sensor based on SAW reflective delay line *1996 IEEE Ultrasonics Symposium. Proceedings* 1996 IEEE Ultrasonics Symposium. Proceedings vol 1 pp 347–50 vol.1

[7] Fachberger R, Bruckner G, Hauser R and Reindl L 2006 Wireless SAW based high-temperature measurement systems *2006 IEEE International Frequency Control Symposium and Exposition* 2006 IEEE International Frequency Control Symposium and Exposition pp 358–67

[8] Floer C, Hage-Ali S, Nicolay P, Chambon H, Zhgoon S, Shvetsov A, Streque J, M'Jahed H and Elmazria O 2020 SAW RFID Devices Using Connected IDTs as an Alternative to Conventional Reflectors for Harsh Environments *IEEE Trans Ultrason Ferroelectr Freq Control* **67** 1267–1274

[9] Maskay A, Hummels D M and Pereira da Cunha M 2018 SAWR dynamic strain sensor detection mechanism for high-temperature harsh-environment wireless applications *Measurement* **126**

[10] Wilson W C, Rogge M D, Fisher B H, Malocha D C and Atkinson G M 2012 Fastener Failure Detection Using a Surface Acoustic Wave Strain Sensor *IEEE Sens. J.* **12** 1993–2000

[11] Oishi M, Hamashima H and Kondoh J 2016 Measurement of cantilever vibration using impedance-loaded surface acoustic wave sensor *Jpn. J. Appl. Phys.* **55** 07KD06

[12] Shu L, Jiang J, Peng B, Wang Y and Liu X 2015 AlN film SAW resonator integrated with metal structure *Electron. Lett.* **51** 379–80

[13] Shu L, Peng B, Cui Y, Gong D, Liu X and Zhang W 2016 High temperature characteristics of AlN film SAW sensor integrated with TC4 alloy substrate *Sens. Actuators Phys.* **249** 57–61

[14] Shu L, Wang X, Li L, Yan D, Peng L, Fan L and Wu W 2019 The investigation of integrated SAW strain sensor based on AlN/TC4 structure *Sens. Actuators Phys.* **293** 14–20

[15] Mengue P, Hage-Ali S, Elmazria O and Zhgoon S 2020 SAW Sensors Directly Integrated onto Industrial Metallic Parts for Manufacturing 4.0 *2020 IEEE International Workshop on Metrology for Industry 4.0 IoT* 2020 IEEE International Workshop on Metrology for Industry 4.0 IoT pp 158–61

[16] Ieki H and Kadota M 1999 ZnO thin films for high frequency SAW devices *1999 IEEE Ultrasonics Symposium. Proceedings. International Symposium (Cat. No.99CH37027)* 1999 IEEE Ultrasonics Symposium. Proceedings. International Symposium (Cat. No.99CH37027) vol 1 pp 281–9 vol.1

[17] Le Brizoual L, Sarry F, Elmazria O, Alnot P, Ballandras S and Pastureaud T 2008 GHz frequency ZnO/Si SAW device *IEEE Trans. Ultrason. Ferroelectr. Freq. Control* **55** 442–50

[18] Floer C, Hage-Ali S, Zhgoon S, Moutaouekkil M, Bartoli F, Mishra H, McMurtry S, Pigeat P, Aubert T, Bou Matar O, Talbi A and Elmazria O 2018 AlN/ZnO/LiNbO3 Packageless Structure as a Low-Profile Sensor for Potential On-Body Applications *IEEE Trans. Ultrason. Ferroelectr. Freq. Control* **65** 1925–32

[19] Elmazria O, Zhgoon S, Le Brizoual L, Sarry F, Tsimbal D and Djouadi M A 2009 AlN/ZnO/diamond structure combining isolated and surface acoustic waves *Appl. Phys. Lett.* **95** 233503

[20] Legrani O, Elmazria O, Zhgoon S, Pigeat P and Bartasyte A 2013 Packageless AlN/ZnO/Si Structure for SAW Devices Applications *IEEE Sens. J.* **13** 487–91

[21] Liu Y, Luo J T, Zhao C, Zhou J, Ahmad Hasan S, Li Y, Cooke M, Wu Q, Ng W P, Du J F, Yu Q, Liu Y and Fu Y Q 2016 Annealing Effect on Structural, Functional, and Device Properties of Flexible ZnO Acoustic Wave Sensors Based on Commercially Available Al Foil *IEEE Trans. Electron Devices* **63** 4535–41

[22] Shvetsov A, Zhgoon S, Antcev I, Bogoslovsky S and Sapozhnikov G 2016 Quartz orientations for optimal power efficiency in wireless SAW temperature sensors *2016 European Frequency and Time Forum (EFTF)* 2016 European Frequency and Time Forum (EFTF) pp 1–4

[23] Hashimoto K 2000 Resonators *Surface Acoustic Wave Devices in Telecommunications: Modelling and Simulation* ed K Hashimoto (Berlin, Heidelberg: Springer) pp 123–61

[24] Saravanakumar K, Senthilkumar V, Sanjeeviraja C, Jayachandran M, Ganesan V, Koizhaiganova R B, Vasudevan T and Lee M S 2008 The influence of substrate temperature on the electrical properties of zno films prepared by the rf magnetron sputtering technique *Nano* **03** 469–76

[25] Khudiar A 2013 Fabrication temperature sensing by using ZnO Nanoparticles *J. THI- QAR Sci. ISSN 1991- 8690* **4** 75

[26] Richa S 2012 Investigation on Temperature Sensing of Nanostructured Zinc Oxide Synthesized via Oxalate Route *J. Sens. Technol.* **2012**

[27] Eun K, Lee K J, Lee K K, Yang S S and Choa S-H 2016 Highly sensitive surface acoustic wave strain sensor for the measurement of tire deformation *Int. J. Precis. Eng. Manuf.* **17** 699–707